Dynamics of Uniformly ^{13}C-Enriched Cell Wall Polysaccharide of *Streptococcus mitis* J22 Studied by ^{13}C Relaxation Rates[†]

Qiuwei Xu and C. Allen Bush*

Department of Chemistry and Biochemistry, University of Maryland—Baltimore County, Baltimore, Maryland 21228

Received May 28, 1996; Revised Manuscript Received August 30, 1996[⊗]

ABSTRACT: We have studied the dynamics of the motion of a complex polysaccharide having seven sugar residues in the repeating subunit and which is a receptor for lectin interaction in the coaggregation of oral bacteria. Measurements of the longitudinal and the rotating frame relaxation rates and the heteronuclear nuclear Overhauser effects were carried out on a uniformly ^{13}C-enriched sample using pulse sequences chosen to minimize the effects of ^{13}C$-^{13}$C coupling and cross relaxation. T_1 and $T_{1\rho}$ measurements both showed single exponential decay for the anomeric carbon atom resonances of the polysaccharide. The results show the polymer to be highly flexible with a hinge at the $(1\rightarrow6)$-linked galactofuranoside residue. Since there is no generally accepted scheme for interpreting polysaccharide dynamics, several different methods of data analysis were used including a reduced spectral density function method as well as several different methods in which a series of isotropically decaying rotational correlation functions are assumed. The different analyses all show that there are differing amounts of internal motion in the different residues of the polysaccharide. One possible interpretation of the data, which uses an extended version of the model-free treatment, indicates that picosecond motion is exhibited to a similar degree by all the residues in addition to a slower motion on the nanosecond time scale whose amplitude is greatest in the hinge region around the $(1\rightarrow6)$-linked galactofuranoside residue in the polysaccharide.

While the question of the conformation and dynamics of complex polysaccharides has received considerable attention, a number of questions remain concerning the nature and extent of conformational exchange. The notion of flexibility is generally recognized to be important at least for certain oligosaccharide linkages (Rutherford et al., 1993; Poppe & van Halbeek, 1992; Maler et al., 1996; Xu et al., 1996a,b). Although it is accepted that exchange can occur among different conformations of the glycosidic linkage, the kinetics of that exchange remains uncertain. NMR[1] relaxation data provide an experimental approach to this question. Directly detected ^{13}C T_1 data have been reported for natural abundance sucrose by McCain and Markley (1986) which were interpreted in terms of motion on the picosecond time scale attributed to sugar puckering. An alternative approach in which ^{13}C T_1 was measured for a series of homologous oligosaccharides was used to show that motion of a polysaccharide can be viewed in terms of a persistence length of some $10-15$ sugar units. Polymers longer than this show the same values of T_1 for the central residues regardless of chain length (Benesi & Brant, 1985; Brant et al., 1995). These directly detected ^{13}C relaxation experiments generally require sufficiently high concentrations of sample that the viscosity of the solution introduces some concentration dependence to the measured relaxation rates.

Indirect detection offers an improvement in the sensitivity of relaxation rate measurements. In relaxation experiments on the small glycoprotein, ribonuclease B, Rutherford et al. (1993) reported T_1 and T_2 for natural abundance ^{13}C. The data showed limited signal to noise at long relaxation delays but were interpreted with the "model-free" formalism of Lipari and Szabo (1982a,b) to show that the oligosaccharide which is covalently tethered to the protein exhibits internal motion on a time scale of approximately 200 ps. Poppe et al. (1994) in experiments on the ganglioside GD1a inserted in a micelle, observed motions of the oligosaccharide on a time scale of about 300 ps superimposed on a tumbling time of 2.8 ns for the micelle. Hricovini and Torri (1995) have reported T_1, T_2, and ^{1}H NOE data for a pentasaccharide from heparin which was interpreted by the model-free formalism to show a complicated internal motion on the time scale of $15-50$ ps.

The recent introduction of isotopic enrichment into proteins with the stable spin $^1/_2$ isotopes, ^{13}C and ^{15}N, has stimulated interest in relaxation rate measurements to study protein dynamics (Peng & Wagner, 1992; Clore et al., 1990b; Kay et al., 1989; Stone et al., 1992). The improvements in the signal to noise ratios brought about by indirect detection and isotopic enrichment have made possible very accurate measurements of the ^{15}N relaxation rates and very sophisticated theoretical treatments which give detailed insight into the internal motions of proteins. While enrichment of proteins with ^{13}C is also common, measurement of relaxation rates in uniformly highly enriched proteins presents some technical challenges in the design of the NMR experiments (Yamazaki et al., 1994).

We have recently reported the preparation of a cell wall polysaccharide from *Streptococcus mitis* J22 which is uniformly ^{13}C labeled (Gitti et al., 1994). We have carried out measurements of NOE and $^3J_{CH}$ for this polymer and have reported molecular modeling studies which establish that it is a rather flexible polysaccharide [Xu & Bush, 1996 (accompanying paper)]. In this paper we report a method for measuring very accurate ^{13}C relaxation rates for the seven

Chart 1: *S. mitis* J22 Polysaccharide (Proposed Lectin-Combining Site Is Underlined.)

$$[\rightarrow 6)\text{Gal}_p\text{NAc } \alpha\text{-}(1\rightarrow3)\text{-Rha}_p \; \beta\text{-}(1\rightarrow4)\text{-Glc}_p \; \beta\text{-}(1\rightarrow6)\text{-}$$
$$\text{Rha } \alpha\text{-}(1\rightarrow2)\text{-}\nearrow$$
$$\mathbf{g}$$
$$\rightarrow\text{Gal}_f \; \beta\text{-}(1\rightarrow6)\text{-}\underline{\text{Gal}_p \; \beta\text{-}(1\rightarrow3)\text{-Gal}_p\text{NAc } \alpha\text{-}}(1 \rightarrow \text{PO}_4^-\text{-}]_n$$

distinct anomeric carbon atoms in the repeating subunit of this polymer along with several different schemes for interpreting the data in terms of polymer dynamics on the picosecond to nanosecond time scale.

MATERIALS AND METHODS

The polysaccharide sample from *S. mitis* J22 was biosynthetically enriched with ^{13}C to a level of approximately 96% according to the procedure described previously (Gitti et al., 1994). The sample was dissolved in 99.96% D$_2$O at a concentration of 7−10 mg/mL at neutral pH without any buffer. The structure of the polysaccharide is (Abeygunawardana et al., 1990) shown in Chart 1.

NMR experiments were carried on a GE-Omega 500 PSG system controlled by Sun Sparc workstation with reverse-detection through an RPT probe at 24.0 °C. The pulse sequences in Figure 1 for measuring ^{13}C T_1, $T_{1\rho}$, and ^{13}C−{^{1}H} NOE were based on the scheme for relaxation rate measurements on uniformly isotope-labeled biopolymers by Yamazaki et al. (1994). The ^{13}C carrier frequency was set within the anomeric carbon region (104−94 ppm), and all ^{13}C pulses were selective for the anomeric carbons with a low power level so that the other carbon atoms, such as C2, were not excited. Therefore, the cross relaxation terms for carbons in uniformly isotope-enriched sample did not contribute to the relaxation decay of anomeric carbons and Hartman−Hahn effect was avoided during the carbon spin-lock time for $T_{1\rho}$ measurements. The proton carrier frequency was 500.132 114 0 MHz with a sweep width of 2564.1 Hz. The proton dimension contained 256 complex data points. The carbon frequency was set in the middle of anomeric carbon chemical shift region (125.770 591 MHz) with a spectral width of 4000.0 Hz. The 90° pulse for carbon was 155 ms. Carbon decoupling during acquisition was carried out with WALTZ-16 with field strength of 1612.9 Hz. The $^1J_{\text{CH}}$ coupling during carbon constant time evolution was removed with a continuous low-power proton pulse. Proton decoupling during the relaxation delay period for R_1 and $R_{1\rho}$ measurements was done with a series of 180° pulses which eliminate the cross correlation between ^{1}H−^{13}C dipolar interaction and ^{13}C CSA or cross correlation between ^{13}C−^{13}C and ^{1}H−^{13}C dipolar interaction. The presaturation of the proton resonances for ^{13}C−{^{1}H} NOE measurement was carried out with a series of proton 120° pulses. The carbon 90° pulse of phase ϕ_3 in the relaxation measurements of T_1 places carbon magnetization along $+z$ and $-z$ on alternate scans to cancel the effect of the carbon longitudinal magnetization at equilibrium (Sklenar et al., 1987). The delay preceding the relaxation delay in the $R_{1\rho}$ measurement aligned magnetization with an offset from the carrier frequency exactly along the orientation of effective B_1 field, and the delay after the relaxation delay returned all the magnetization to the horizontal plane. The data matrices contained 32 complex data blocks and 64 scans per block in the R_1 and NOE data and 128 scans per block in the $R_{1\rho}$

data. The delays for the R_1 measurement varied between 10 and 400 ms, and those for the $R_{1\rho}$ measurement varied between 10 and 120 ms. The carbon carrier frequency was set at varying values close to individual anomeric carbon resonances for the $R_{1\rho}$ measurements and the relaxation rate measurements were repeated by varying carbon carrier frequency, power level, and relaxation delay to avoid artifacts and to assess experimental reproducibility. NOE measurements were done by acquiring two spectra with and without proton presaturation during pulse delay (2.5 s).

The NMR data were processed with Felix 2.30 (Biosym) on a Silicon Graphics Indigo workstation. The proton dimension was apodized with a 90°-shifted sine-bell function and then zero-filled to 1024 points before Fourier transformation. The data along the carbon dimension were apodized with a 90°-shifted sine-bell function and zero-filled to 128 points before Fourier transformation. The peak height was read from each properly phased cross peak. R_1 and $R_{1\rho}$ data were fitted to a two-parameter exponential function shown by eqs 1 and 2 with software based on nonlinear least-squares data fitting using the Levenberg−Marquardt algorithm (Press et al., 1989).

$$I(T) = 2I_0 \exp^{-R_1 T} \tag{1}$$

$$I(T) = I_0 \exp^{-R_{1\rho} T} \tag{2}$$

^{13}C−{^{1}H} NOE values were obtained from the peak ratios of spectra with and without proton saturation. There was little difference in the relaxation rate values when either peak height or peak volume was used.

The experimental R_1, $R_{1\rho}$, and ^{13}C−{^{1}H} NOE data were analyzed in two different ways. In the first method, the reduced spectral density function was used according to methods described by Farrow et al. (1995), by Ishima and Nagyama (1995), and by Lefevre et al. (1996). An analysis was also done using the "model-free" formalism which assumes that the rotational correlation function is composed of a small number of exponentially decaying components (Lipari & Szabo, 1982a,b; Clore et al., 1990a,b). The data fitting for the model-free formalism was carried out with a conjugate gradient method on the following merit function, χ_2 (Press et al., 1989).

$$\chi_2 = k_1[R_1(\text{calc}) - R_1(\text{expt})]^2 + k_2[R_{1\rho}(\text{calc}) - $$
$$R_{1\rho}(\text{expt})]^2 + k_3[\text{NOE(calc)} - \text{NOE(expt)}]^2 \tag{3}$$

In eq 3, k_1, k_2, and k_3 are coefficients adjusted to facilitate analysis of the experimental data. The parameters describing the molecular motion in the model-free analysis were adjusted and χ_2 minimized with $k_1 = 1.0$, $k_2 = 1.0$, and $k_3 = 0.0$. The calculated NOE was monitored to assure good agreement with experimental values. This procedure was followed to avoid trapping by barriers in this nonlinear fitting.

Our analysis is based on theoretical calculation of the R_1, $R_{1\rho}$ and ^{13}C−{^{1}H} NOE data for the anomeric ^{13}C resonances of the polysaccharide following Clore et al. (1990a) and Peng and Wagner (1992). The relaxation rate R_1, which we have measured for the anomeric ^{13}C resonances, includes all the autorelaxation terms ($\rho_{\text{C1,H1}}$ and $\rho_{\text{C1,C2}}$), but does not contain the cross relaxation term $\sigma_{\text{C1,C2}}$ because carbon excitation was selective for only the anomeric carbons, and does not

FIGURE 1: Pulse sequences. The delay for coherence transfer between ^{1}H and ^{13}C was set according to a $^1J_{CH}$ value of 165 Hz ($\tau_a = 1.465$ ms, $\tau_b = 3.03$ ms, $\tau_c = 1.415$ ms). The carbon constant evolution time (δ) was set using $^1J_{CC} = 45$ Hz. The delays between proton 180° pulses during the relaxation delay period for R_1 and $R_{1\rho}$ measurements were set as 2.0 ms and 1.0 ms, respectively. The presaturation for ^{13}C−\{^{1}H\} NOE measurement was carried out with proton 120° pulses spaced at 2.4 ms. Residual magnetization was removed in R_1 and $R_{1\rho}$ measurements by purge pulses along x for 1.0 ms and y for 0.5 ms, and a homospoil pulse of 0.5 ms. The phases are as follows: $\phi_1 = x$; $\phi_2 = (x,y,-x,-y)$; $\phi_3 = 4(y), 4(-y)$; receiver $= 2(x,-x), 2(-x,x)$. The phases in Figure 1b include $\phi_4 = 8(x), 8(-x)$, and in Figure 1c the receiver phase $= (x,-x)$.

contain $\sigma_{H1,C1}$ due to proton saturation during the relaxation delay (Yamazaki et al., 1994). Therefore the dipolar contributions of H1 and of C2 to the relaxation of the anomeric carbon atom are formally identical. Chemical shift anisotropy (CSA) is included in the last term of the R_1 and $R_{1\rho}$ expressions. It is important to recognize that R_1 contains $J(0)$ as a result of ^{13}C−^{13}C autorelaxation, and this term, although small compared with other relaxation terms in R_1, increases with increasing rotational correlation time.

$$R_1 = \sum_{i,j}(d^2/r_{i,j}^6)[J(\omega_i - \omega_j) + 3J(\omega_j) +$$

$$6J(\omega_i + \omega_j)] + (\Delta^2\omega_C^2/3)J(\omega_C) \quad (4)$$

$$R_{1\rho} = \sum_{i,j}(d^2/r_{i,j}^6)\{4\sin^2(\beta)J(\omega_e) + 2[\sin^4(\beta/2)J(\omega_i -$$

$$\omega_j + \omega_e) + \cos^4(\beta/2)J(\omega_i - \omega_j - \omega_e)] +$$

$$6[\sin^4(\beta/2)J(\omega_i - \omega_e) + \cos^4(\beta/2)J(\omega_j - \omega_e)] +$$

$$3\sin^2(\beta)[J(\omega_i + \omega_e) + J(\omega_i - \omega_e)] +$$

$$12[\cos^4(\beta/2)J(\omega_i + \omega_j + \omega_e) + \sin^4(\beta/2)J(\omega_i +$$

$$\omega_j - \omega_e)]\} + (\Delta^2\omega_C^2/3)\{(^2/_3)\sin^2(\beta)J(\omega_e) +$$

$$[\sin^4(\beta/2)J(\omega_C - \omega_e) + \cos^4(\beta/2)J(\omega_C - \omega_e)]\} \quad (5)$$

$$\text{NOE} = 1 + \sigma_{H,C}/\rho_C \quad (6)$$

$$\sigma_{H,C} = (\gamma_H/\gamma_C)(d^2/r_{i,j}^6)[6J(\omega_H + \omega_C) - J(\omega_H - \omega_C)] \quad (7)$$

For the case discussed here, $\rho_C = R_1$ in eq 6.

In our application, in the eqs 4 and 5 for R_1 and $R_{1\rho}$, the terms in the summation over i and j include C1 for j and both H1 and C2 for i. The values of the constants in eqs 4−6 are the following: $h = 6.626 \times 10^{-27}$ erg s, $\gamma_H = 2.6752 \times 10^4$ gauss^{-1} s^{-1}, $\gamma_C = 6.728 \times 10^3$ gauss^{-1} s^{-1}, $r_{CH} = 1.09 \times 10^{-8}$ cm, $r_{CC} = 1.515 \times 10^{-8}$ cm. The constant $d^2 = 0.1 (\gamma_i\gamma_j h/2\pi)^2$.

$\omega_e^2 = \omega_1^2 + \delta^2$, where $\omega_1 = 2\pi H_1$ and H_1 is the proton B_1 spin-lock field strength in Hz. δ is the offset from the spin-lock carrier frequency. Δ is the chemical shift anisotropy of ^{13}C (CSA) which is taken as 50.0 ppm (Bovey, 1980; Hricovini & Torri, 1995). The spin-locking tilt angle is β, and $\sin\beta = \omega_1/\omega_e$.

The uncertainties in spectral density function analysis and model-free formalism as obtained from fitting experimental data were estimated with Monte Carlo simulation. The measured experimental values and their error ranges were assumed as the mean and standard deviation of a Gaussian distribution. The relaxation rates were calculated from each set of 50 000 randomly generated parameters in the spectral

T1 exponential decay of ^{13}C1 of the residue c

T1ρ exponential decay of ^{13}C1 of the residue c
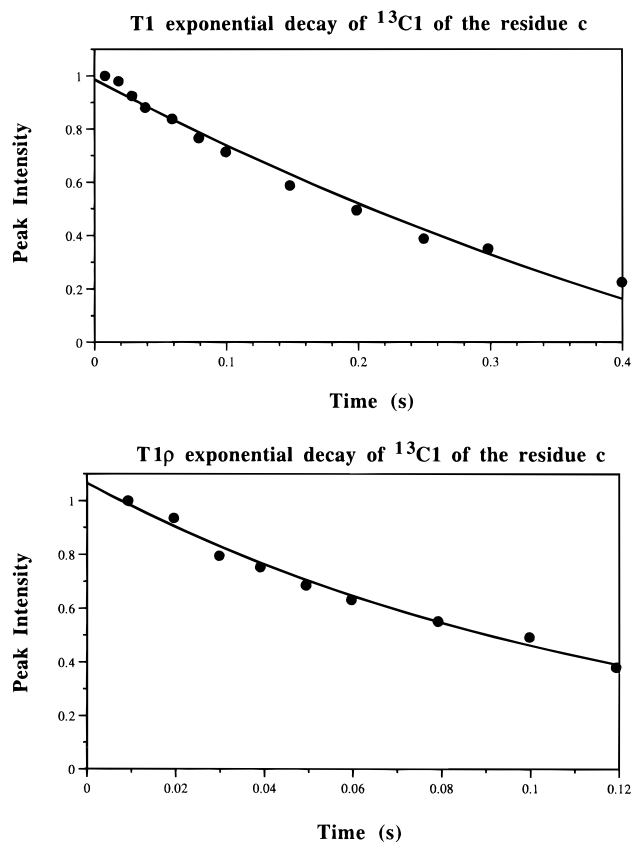
FIGURE 2: T_1 and $T_{1\rho}$ of the anomeric ^{13}C resonances of residue **c**.

Table 1: Experimental Data of ^{13}C Relaxation Rates

residue	R_1 (s^{-1})^a	$R_{1\rho}$ (s^{-1})^a	NOE^a	$R_{1\rho}/R_1$
a	1.22	10.33	1.08	8.47
b	1.28	11.43	1.05	8.93
g	1.32	10.75	1.03	8.14
c	1.11	7.97	1.26	7.18
d	1.10	5.26	1.20	4.78
e	1.19	7.06	1.14	5.93
f	1.16	9.17	1.19	7.90

^{a} The experimental error of the measurements is about 10% of the values as indicated by the error bars in Figures 3 and 4.

RESULTS AND DISCUSSION

The dilute polysaccharide used in these experiments eliminates problems which arise from dependence of relaxation rates on concentration which has been encountered in some previous polysaccharide studies. Nevertheless, the signal to noise ratio for the relaxation data is excellent with a ^{13}C-enriched sample when compared to natural abundance polysaccharides. The data illustrated in Figure 2 show little scatter, even at long delay times, and the fit to a single exponential decay is excellent. Table 1 and Figures 3 and 4 show that there are small differences in the T_1 and NOE data among the signals for the seven anomeric carbon atoms. While the differences are only slightly larger than the error bars for R_1 and NOE, there are very significant differences in the $R_{1\rho}$ data in Table 1 and in Figure 3b. Variations of
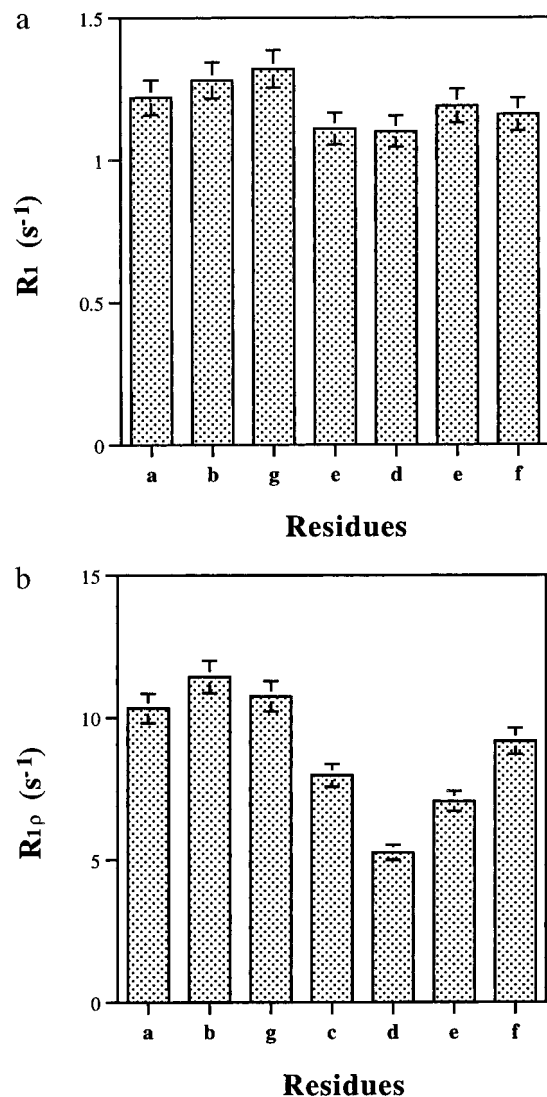
FIGURE 3: Plots of R_1 (a) and $R_{1\rho}$ (b) for the anomeric ^{13}C signals of the different residues.
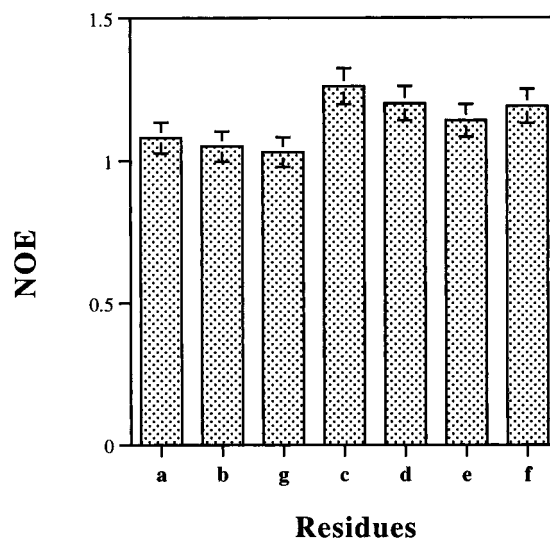
FIGURE 4: Plot of NOE for the anomeric ^{13}C signals of the different residues.

the carbon carrier frequency have little influence on the measured values of R_1 and NOE. The values of $R_{1\rho}$ were measured with the carbon carrier frequency set no more than 250 Hz away from the ^{13}C resonances, and the exact carbon

carrier frequency offsets were taken into account in the data analysis as will be described below.

One method for analysis of relaxation data, which requires the determination of additional relaxation rates, is the full spectral density function method of Peng and Wagner (1992). With three sets of relaxation rates as reported in this work, an alternative reduced spectral density function analysis is possible (Lefevre et al., 1996; Ishima & Nagayama, 1995; Farrow et al., 1995). Equations 4−7 can be simplified with the assumption of the form of eq 8 for $J(\omega)$.

$$J(\omega) = \lambda_1/\omega^2 + \lambda_2 \qquad (8)$$

The first and second terms in eq 8 represent contributions to $J(\omega)$ from overall tumbling and from internal motion, respectively (Farrow et al., 1995). With the inclusion of eq 8, eqs 4−7 can be reduced to eqs 9−11 in which three new frequencies, ω_p, ω_q, and ω_r are defined.

$$6J(\omega_H + \omega_C) - J(\omega_H - \omega_C) = 5J(\omega_p) \qquad (9)$$

$$6J(\omega_H + \omega_C) + J(\omega_H - \omega_C) = 7J(\omega_q) \qquad (10)$$

$$6J(\omega_H) + 6J(\omega_H + \omega_C) + J(\omega_H - \omega_C) = 13J(\omega_r) \qquad (11)$$

The new forms of eqs 9−11 are recast with appropriate gyromagnetic ratios of ^{1}H and ^{13}C.

$$6J(\omega_H + \omega_C) - J(\omega_H - \omega_C) = 5J(1.563\omega_H) \qquad (12)$$

$$6J(\omega_H + \omega_C) + J(\omega_H - \omega_C) = 7J(1.116\omega_H) \qquad (13)$$

$$6J(\omega_H) + 6J(\omega_H + \omega_C) + J(\omega_H - \omega_C) = 13J(1.058\omega_H) \qquad (14)$$

Equations 12−14 are analogous to eq 11 of Farrow et al. (1995) with ^{13}C substituted for ^{15}N. In order to simplify eq 5 to accommodate the reduced spectral density function analysis, it is necessary to introduce further simplifications into the treatment of the $R_{1\rho}$ data. Because the offset of the anomeric carbon resonance frequency from the carrier is small compared to the B_1 field strength, the rotating frame is tilted close to the x,y plane. Therefore $\sin^2\beta \approx 1.0$ and $\sin^4\beta/2 + \cos^4\beta/2 \approx 0.5$ in eq 5 and ω_e is set to 0. The validity of an additional assumption, that relaxation of C1 by C2 can be neglected, will be discussed below. In this particular system the ^{13}C−^{13}C autorelaxation is only a few percent of the total relaxation. With these approximations, eq 5 may be written as

$$R_{1\rho} = (d^2/r_{C,H}^6)\{4J(0) + 3J(\omega_C) + 13J(1.058\omega_H)\} + (\Delta^2\omega_C^2/3)\{(^2/_3)J(0) + (^1/_2)J(\omega_C)\} \qquad (15)$$

For this situation, eq 15 becomes the same as the formula for T_2 relaxation. Similarly, eqs 4 and 7 can be recast using eqs 12−14 in eqs 16 and 17, respectively.

$$R_1 = (d^2/r_{C,H}^6)[3J(\omega_C) + 7J(1.116\omega_H)] + (\Delta^2\omega_C^2/3)J(\omega_C) \qquad (16)$$

$$\sigma_{H,C} = (\gamma_H/\gamma_C)(d^2/r_{C,H}^6)[5J(1.563\omega_H)] \qquad (17)$$

Equations 15−17 involve the spectral density sampled at ω_C,

Table 2: Reduced Spectral Density Function Analysis (Method 1) (in s/rad)

residue	$J(0)$ $(\times10^{-9})$	$J(\omega_C)$ $(\times10^{-10})$	$J(1.058\omega_H)$ or $J(1.116\omega_H)$ or $J(1.563\omega_H)$ $(\times10^{-12})$
a	1.06 ± 0.01	1.84 ± 0.13	2.29 ± 1.87
b	1.18 ± 0.01	1.95 ± 0.08	1.50 ± 2.06
g	1.09 ± 0.01	2.03 ± 0.07	0.93 ± 0.98
c	0.79 ± 0.01	1.56 ± 0.07	6.76 ± 2.17
d	0.48 ± 0.01	1.59 ± 0.07	5.15 ± 2.08
e	0.68 ± 0.01	1.75 ± 0.08	3.90 ± 1.81
f	0.92 ± 0.01	1.68 ± 0.07	5.16 ± 1.77

at 0, and at three frequencies close to and above ω_H. The situation discussed here for ^{13}C differs somewhat from that of ^{15}N relaxation treated by Farrow et al. (1995) in that the three frequencies differ more substantially from ω_H as a result of the difference in sign and magnitude of the magnetogyric ratios of the heteronuclei. Thus, two different approaches are taken to reduce the five spectral density function values in eqs 15−17 to three needed for our analysis. It is necessary to assume a description of the shape of the decay of the spectral density function at and above the proton frequency, ω_H. Although the exact values of spectral density function will be greatly influenced by the nature of the assumptions, we will focus on the correlation of the internal motion on the nanosecond scale with the spectral density function values at zero frequency. These values are less sensitive to the details of the assumptions, as will be seen in the following. In the first case we assume that $J(\omega_H)$ is essentially constant near ω_H. Then $J(1.116\omega_H)$ and $J(1.563\omega_H)$ may be replaced with $J(1.058\omega_H)$. The calculated $J(0)$, $J(\omega_C)$, $J(1.058\omega_H)$, $J(1.116\omega_H)$, and $J(1.563\omega_H)$ derived by this method are listed in Table 2.

A second approach may provide a better description of the decay of the shape of $J(\omega)$ at or beyond the proton frequency. The assumption that $J(\omega)$ decays like $1/\omega^2$ is equivalent to the assumption that a single exponentially decaying rotational correlation function dominates in the region of ω_H. Under this assumption $J(1.116\ \omega_H)$ and $J(1.563\omega_H)$ can be estimated from the relation $J(\epsilon\omega_H) = (1.058/\epsilon)^2 \times J(1.058\omega_H)$ where $\epsilon = 1.116$ and 1.563. The calculated $J(0)$, $J(\omega_C)$, $J(1.058\omega_H)$, $J(1.116\omega_H)$, and $J(1.563\omega_H)$ derived according to this method are listed in Table 3 and plotted in Figure 5.

The results of the two treatments summarized in Tables 2 and 3 are quite different for $J(\omega)$ in the region of the proton frequency, and show a slight difference for the carbon frequency but very similar values for $J(0)$. The uncertainties in spectral density function values at high frequency (at and beyond the proton frequency) are much larger than those at low or zero frequency. The values of $J(0)$ derived from the reduced spectral function analysis are reliable and informative concerning the internal motion on the nano or subnanosecond time scale. Figure 5 illustrates graphically the data of Table 3 showing that $J(0)$ varies among the residues of the polymer subunit in a similar manner to that of $R_{1\rho}$.

One may raise the objection to the analysis described above that it is not so appropriate for ^{13}C as it is for ^{15}N relaxation for which it was originally derived. It is possible to present an alternative interpretation of our data using the treatment of Lipari and Szabo (1982a,b) which provides a more concrete description of the internal motion including both time and amplitudes. This model, which is known as

Table 3: Reduced Spectral Density Function Analysis (Method 2) (in s/rad)

residue	$J(0)$ $(\times 10^{-9})$	$J(\omega_C)$ $(\times 10^{-10})$	$J(1.058\omega_H)$ $(\times 10^{-12})$	$J(1.116\omega_H)$ $(\times 10^{-12})$	$J(1.563\omega_H)$ $(\times 10^{-12})$
a	1.05 ± 0.01	1.79 ± 0.08	4.99 ± 4.58	4.49 ± 4.12	2.29 ± 2.10
b	1.18 ± 0.01	1.92 ± 0.13	3.27 ± 4.06	2.94 ± 3.65	1.50 ± 1.86
g	1.09 ± 0.01	2.00 ± 0.08	2.02 ± 1.06	1.82 ± 1.44	0.93 ± 0.73
c	0.79 ± 0.01	1.41 ± 0.12	14.75 ± 4.24	13.26 ± 3.82	6.76 ± 1.94
d	0.47 ± 0.01	1.47 ± 0.11	11.25 ± 4.52	10.11 ± 4.07	5.15 ± 2.07
e	0.67 ± 0.01	1.67 ± 0.09	8.52 ± 4.93	7.66 ± 4.43	3.90 ± 2.26
f	0.91 ± 0.01	1.56 ± 0.06	11.27 ± 4.20	10.13 ± 3.78	5.16 ± 1.92
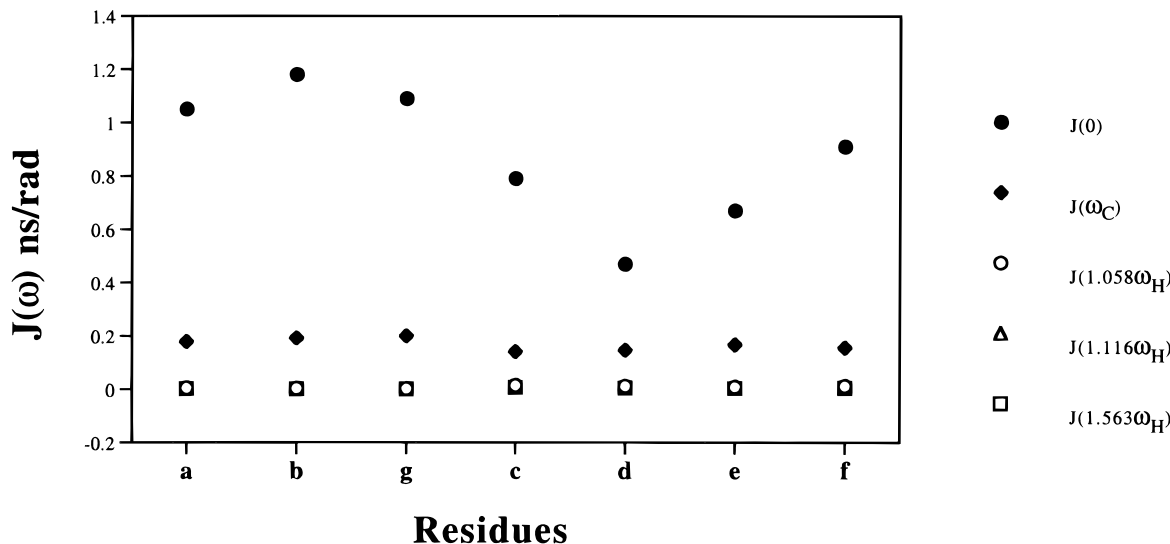
FIGURE 5: Plot of $J(\omega)$ for the anomeric ^{13}C signals of the different residues.

Table 4: Data from Individual Residue Fitting to Lipari−Szabo Model (Eq 18)

residue	τ_R (ns)	τ_e (ns)	S^2	R_1 (s^{-1})	$R_{1\rho}$ (s^{-1})	NOE
a	4.6 ± 0.05	0.002 ± 0.001	0.42 ± 0.02	1.21	10.3	1.17
b	4.7 ± 0.05	0.001 ± 0.000	0.45 ± 0.02	1.27	11.4	1.16
g	4.4 ± 0.05	0.0006 ± 0.000	0.46 ± 0.02	1.33	10.7	1.15
c	4.1 ± 0.05	0.0008 ± 0.0002	0.36 ± 0.01	1.12	7.97	1.16
d	3.2 ± 0.06	0.0008 ± 0.0002	0.29 ± 0.01	1.10	5.25	1.17
e	3.6 ± 0.06	0.0001 ± 0.0000	0.36 ± 0.02	1.21	7.04	1.15
f	4.4 ± 0.05	0.001 ± 0.000	0.39 ± 0.01	1.16	9.17	1.16

Table 5: Data from Fitting to Lipari−Szabo Model with $\tau_R = 4.7$ ns (Eq 18)

residue	τ_e (ns)	S^2	R_1 (s^{-1})	$R_{1\rho}$ (s^{-1})	NOE
a	0.006 ± 0.002	0.41 ± 0.02	1.22	10.3	1.26
b	0.002 ± 0.001	0.45 ± 0.02	1.28	11.4	1.17
g	0.012 ± 0.003	0.42 ± 0.02	1.32	10.8	1.34
c	0.017 ± 0.003	0.31 ± 0.02	1.11	7.97	1.54
d	0.032 ± 0.002	0.19 ± 0.02	1.10	5.25	2.04
e	0.028 ± 0.003	0.27 ± 0.02	1.19	7.06	1.81
f	0.010 ± 0.003	0.37 ± 0.02	1.16	9.17	1.36

the model-free treatment, assumes a series of exponentially decaying isotropic rotational correlation functions. There are several different versions of this treatment available, which differ in the number of exponentially decaying components and in assumptions about their rates. In the simplest formulation (Lipari & Szabo, 1982a,b), an overall tumbling described by τ_R is modulated by a very fast internal rotation τ_e. In order to survey the range of overall tumbling times (τ_R) which best fit the relaxation data for each individual residue, we minimized the merit function shown by eq 3 with the simple isotropic diffusion Lipari−Szabo model described by eq 18 for each individual anomeric carbon resonance.

$$J(\omega) = S^2\tau_R/(1 + \omega^2\tau_R^2) + (1 - S^2)\tau/(1 + \omega^2\tau^2) \quad (18)$$

In eq 18, $\tau = \tau_R\tau_e/(\tau_R + \tau_e)$. Values of S^2, τ_R, and τ_e were derived using eq 3 to fit R_1 and $R_{1\rho}$ with an iterative adjustment to fit the NOE data. The estimate of τ_e in Table 4 is crude since the data fit is not very sensitive to this parameter. While the fit of Table 4 to the data is satisfactory, the use of different τ_R values for different residues is not fully consistent with the theory in which a single molecular tum-

bling rate is modulated by faster internal motion. The overall tumbling times τ_R for residues **a**, **b**, **g**, and **f** are similar, but those for residues **d**, **e**, and **c** are substantially faster.

For this reason, we have attempted to fit the data to a single overall tumbling time, τ_R, modulated by internal motions which differ among the residues. The overall tumbling time of residue **b**, which is the largest from Table 4, is selected and the fitting was accomplished by minimizing the merit function χ^2 shown in eq 3. The result of this iterative fitting of an internal motion time τ_e and order parameter for each individual residue according to eq 18 is shown in Table 5.

The order parameters of internal motion indicate that the residue **d** (galactofuranose) has the largest internal motion amplitude and residue **b** is relatively restricted in its internal motion. All the residues show much smaller order parameters than the values found for rigid biopolymers. The internal motion is on the time scale from one to tens of picoseconds, which is 2−3 orders of magnitude smaller than the overall tumbling time, τ_R. However, the fitting is not satisfactory since the NOE values calculated with the parameters of this model for internal motion are larger than the experimental values.

Table 6: Data from Fitting to Clore's Model with $\tau_R = 4.7$ ns (Eq 20)

residue	S_f^2	S_s^2	τ_s (ns)	R_1 (s^{-1})	$R_{1\rho}$ (s^{-1})	NOE
a	0.43 ± 0.02	0.96 ± 0.03	1.20 ± 0.35	1.22	10.3	1.15
b	0.46 ± 0.01	0.99 ± 0.07	0.30 ± 0.09	1.28	11.4	1.16
g	0.45 ± 0.01	0.94 ± 0.03	1.10 ± 0.32	1.32	10.8	1.16
c	0.35 ± 0.01	0.87 ± 0.04	1.10 ± 0.32	1.11	7.97	1.19
d	0.29 ± 0.01	0.63 ± 0.05	1.00 ± 0.29	1.10	5.25	1.27
e	0.34 ± 0.01	0.75 ± 0.04	1.10 ± 0.32	1.19	7.06	1.22
f	0.39 ± 0.01	0.93 ± 0.03	1.20 ± 0.35	1.16	9.17	1.16

Although one possible explanation for the unsatisfactory fit of Table 5 could be anisotropic tumbling of the polysaccharide subunit (Schurr et al., 1994; Hricovini & Tori, 1995), we have some evidence indicating that anisotropy is not significant. In model building based on $^3J_{CH}$ data and NOE data for the polysaccharide of *S. mitis* J22, we have observed that the orientation of the C1–H1 vectors of residues **a**, **b**, **g**, and **f** are quite different, so it is likely that these vectors would differ in their orientation with respect to the principal axis of any anisotropic motion [Xu & Bush, 1996 (accompanying paper)]. Nevertheless, the τ_R values of these residues are similar and the most pronounced differences are seen for the galactofuranoside, residue **d** (Table 4). In addition, ^{1}H NOE studies on an isolated heptasaccharide gave values which are very similar to NOE data for the intact polysaccharide, providing evidence that the contribution of anisotropic motion in the polysaccharide is not important (Xu et al., 1996b). Therefore, we conclude that the differences in τ_R among the residues of the polysaccharide do not arise from anisotropy.

Other possible explanations for the unsatisfactory fit to the model include slow chemical exchange processes and multiple modes of internal motion on different time scales. The present data provide no evidence for slow exchange processes, and we were unable to reconcile the data of Table 5 with any reasonable assumptions regarding exchange. But Clore et al. (1990a,b) proposed a model which is an extension of the original simple Lipari–Szabo model and which includes three different types of exponentially decaying rotational correlations. This formalism includes two different internal motions, one fast characterized by τ_f and one slower motion characterized by τ_s, which are superimposed on the overall molecular tumbling. Equation 19 describes $J(\omega)$ for this model, and a reduced formalism is given in eq 20 which is normally used because the second term in eq 19 is small as a result of small τ_f.

$$J(\omega) = S^2\tau_R/(1 + \omega^2\tau_R^2) + (1 - S_f^2)\tau_f'/(1 + \omega^2\tau_f'^2) + (S_f^2 - S^2)\tau_s'/(1 + \omega^2\tau_s'^2) \quad (19)$$

$$J(\omega) = S^2\tau_R/(1 + \omega^2\tau_R^2) + (S_f^2 - S^2)\tau_s'/(1 + \omega^2\tau_s'^2) \quad (20)$$

In eqs 19 and 20, $\tau_i' = \tau_R\tau_i/(\tau_R + \tau_i)$, with $i =$ f,s and $S^2 = S_f^2 S_s^2$. The results of fitting our data to eq 20 by minimizing χ^2 in eq 3 are listed in Table 6 and a bar plot of the order parameters for the seven residues of the repeating subunit of the polysaccharide is shown in Figure 6.

The rates calculated with eq 20 in Table 6 fit rather well with the experimental data of Table 1. While the fit does not guarantee that this model correctly describes the motions of the polysaccharide, it does offer a plausible framework
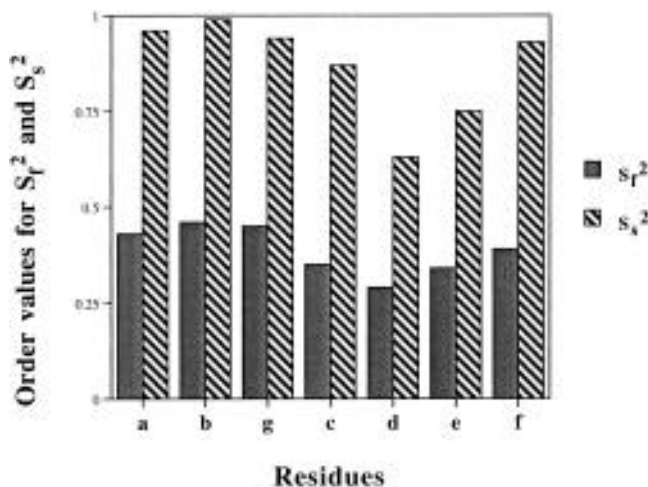
FIGURE 6: Plot of the order parameters for fast (picosecond time scale, S_f) and slow (nanosecond time scale, S_s) internal motion for the anomeric ^{13}C signals of the different residues.

for describing possible motions. The order parameters (S^2) of internal motion calculated from the product of S_f^2 and S_s^2 are similar to the order parameters in Table 5. However, this formalism implies another internal motion on the nanosecond time scale with an order parameter close to 1.0 for residue **b** but much smaller for residues **c**, **d**, and **e**.

We have also used the total error function (eq 21) (Dellwo & Wand, 1989) to evaluate the quality of data fitting to model-free formalism by Clore et al. (1990).

$$E = (1/kN)\sum_N \{(T_1^{calc} - T_1^{meas})^2/(\Delta T_1)^2 +$$
$$(T_{1\rho}^{calc} - T_{1\rho}^{meas})^2/(\Delta T_{1\rho})^2 +$$
$$(NOE^{calc} - NOE^{meas})^2/(\Delta NOE)^2\} \quad (21)$$

In eq 21, the summation extends over all N residues and k denotes the number of measured variables used in the data fit. The value of E for fitting the results in Table 6 is 0.157, which indicates that this is an excellent data fit to the model of Clore et al. (1990b) compared to the fitting for proteins.

It is clear from the data analysis according to the formalisms of Lipari and Szabo (1982a,b) and of Clore et al. (1990a) that the order parameters generally do not depend strongly on the choice of model. The order parameter S^2 for residue **d** is the smallest and for residue **b** is the largest among the seven residues. Regardless of the choice of model, the residues fall into two groups with residues **a**, **b**, **g**, and **f** showing less motion and residues **c**, **d**, and **e** being more mobile.

According to the model of Clore et al. (1990a,b), two internal motions are necessary, one on a picosecond time scale and the other on a nanosecond time scale, in order to properly account for R_1, $R_{1\rho}$, and ^{13}C–{^{1}H} NOE for all the residues. A possible interpretation of this result is that the fast motion contains sugar puckering motions which have been described in molecular dynamics simulations of saccharides (Brady, 1990; Hadjuk et al., 1993), but examination of data in the literature shows that the fast motion cannot be completely explained by sugar puckering. In an analysis of relaxation data on sucrose using the treatment of Lipari and Szabo (1982a,b), McCain and Markley (1986) found order parameters $S^2 = 0.89$ and a recent study of cyclodextrins by Kowalewski and Widmalm (1994) found values of the

order parameter $S^2 = 0.81-0.86$. These values are substantially larger than those reported in Tables 4−6. Therefore it is likely that there are some motions of the glycosidic bonds of the polysaccharide included in the fast motion. Curiously these motions are similar for all the residues of the polysaccharide but they have slightly greater amplitude for residue **d**, the galactofuranoside.

There is a clear variation of dynamics as a function of individual residue with the most significant deviation of both the slow and the fast internal motion from the average occurring for the residues **b**, **g**, and **d**. The motions around residues **b** and **g** are more restricted, and the motions of residue **d** have larger amplitude. It is important to note that this conclusion does not rest only on the model-free analysis and it is also implied by the reduced spectral density analysis of Table 3 and Figure 5. The different dynamics of these residues are presumably the result of structural variation at these two sites. Polysaccharide modeling based on NOESY and $^3J_{CH}$ data shows that around residues **b** and **g** (the antigenic site) the conformational space is very crowded and local conformational exchange is hindered [Xu & Bush, 1996 (accompanying paper)]. The increased dynamic flexibility around residue **d** may result from the (1→6)-linkages and from the puckering of the galactofuranoside ring.

CONCLUSIONS

Most of the NMR relaxation rate data reported in the recent literature have focused on ^{15}N with rather less attention on ^{13}C. In the latter case, problems due to $^{13}C-^{13}C$ interaction arise for uniformly highly enriched samples (Yamazaki et al., 1994). The use of ^{13}C pulses which are selective for the anomeric carbon resonance region of the polysaccharide NMR spectrum along with the pulse sequences proposed by Yamazaki et al. (1994) avoid these problems and give good single exponential decays for T_1 and $T_{1\rho}$ (Figure 2). We were not able to measure T_2 for our sample but the use of on-resonance $T_{1\rho}$ provided information of the same type which is critical to the successful interpretation of the relaxation rate data in terms of internal motion on the nanosecond time scale. Our analysis of the data with the reduced spectral density function neglected C1−C2 autorelaxation, but the effect can be estimated if we assume that $J(\omega)$ derived from the model-free treatment is approximately correct. In eqs 4 and 5 j and i are taken as C1 and C2, and using $J(\omega)$ calculated according to either eq 18 (Table 5) or to eq 20 (Table 6) we can calculate the expected contributions to both R_1 and to $R_{1\rho}$ resulting from $^{13}C-^{13}C$ autorelaxation. The contributions range from 0.03 s^{-1} for residue **d** to 0.12 s^{-1} for residue **b**. These effects, which amount to only 1−2% of the total R_1 or $R_{1\rho}$ for our example, could become substantial for slower rotational correlation times. The effects of chemical shift anisotropy, which can be significant for ^{15}N, are less important for the ^{13}C case (Jarvet et al., 1996).

Since little is known about the detailed dynamics of polysaccharides, interpretation of relaxation rate data in terms of polysaccharide dynamics is rather uncertain and almost any method chosen is subject to some criticism. The reduced spectral density method requires some questionable assumptions concerning the shape of the $J(\omega)$ curve in the region of ω_H. But, independent of those assumptions, the data appear to indicate that $J(0)$ is smaller for the galactofura-

noside residue, **d**, than for the other residues in the polymer, implying that internal motion, presumably on the picosecond to nanosecond time scale, is greater for that residue. This conclusion is not greatly influenced by the method of data treatment and rests on the observed $T_{1\rho}$ data which show slower rates for residue **d**. Other methods of interpretation based on the model-free approach of Lipari and Szabo (1982a,b) assume a series of isotropic exponentially decaying rotational correlation functions. Application to this problem requires some explicit assumptions about the nature of these discrete relaxation times. Most previous applications of these methods have been to globular proteins for which the assumption of an overall rotational correlation time, τ_R, modulated by one or more distinct internal motions is physically reasonable. Appropriation of this type of model for use in polysaccharides may be questioned since the meaning of τ_R for such a system is not entirely clear. It is our interpretation that τ_R (4.7 ns) used in the construction of Tables 5 and 6 refers to the approximately isotropic motion of a unit about the size of the "persistence length" discussed by Brant et al. (1995). For this polymer, this unit must contain approximately 10 sugar residues. In spite of some justifiable criticism of our model-free treatment of the data, the results do agree with the reduced spectral density method on the matter of the greater mobility of the residues in the hinge region around the galactofuranoside, **d**. The model-free treatment further suggests that picosecond motions of the glycosidic linkages are more uniformly distributed along the polysaccharide and that the motions of the hinge region on the time scale of a few nanoseconds are responsible for the great flexibility of the polymer.

It is quite possible there could be internal motions of this polysaccharide on a time scale longer than τ_R which we have failed to detect. In fact there are almost certainly motions of the larger blocks of residues which are responsible for the observation that relaxation rates measured for a series of oligosaccharides become independent of chain length at about 10−15 residues (Brant et al., 1995). Such motions, which are subject to a substantial viscous drag by the solvent, may be on time scales of microseconds to milliseconds and might not be detected in our experiments. Slower internal motions of this type have been referred to as slow exchange phenomena (Clore et al., 1990b). They may be most effectively detected by $R_{1\rho}$ measurements as a function of carrier offset and B_1 field strength (Markus et al., 1996; Akke & Palmer, 1996).

REFERENCES

Abeygunawardana, C., Bush, C. A., & Cisar, J. O. (1990) *Biochemistry 29*, 234−248.

Akke, M., & Palmer, A. G. (1996) *J. Am. Chem. Soc. 118*, 911−912.

Benesi, A. J., & Brant, D. A. (1985) *Macromolecules 18*, 1109−1116.

Bovey, F. A. (1980) *Nuclear Magnetic Resonance Spectroscopy*, Academic Press, New York.

Brady, J. (1990) *Adv. Biophys. Chem. 1*, 155−202.

Brant, D., A., Liu H. S., & Zhu, Z. S. (1995) *Carbohydrate Res. 278*, 11−26.

Clore, G. M., Szabo, A., Bax, A., Kay, L. E., Driscoll, P. C., & Gronenborn, A. M. (1990a) *J. Am. Chem. Soc. 112*, 4989−4991.

Clore, G. M., Driscoll, P. C., Wingfield, P. T., & Gronenborn, A. M. (1990b) *Biochemistry 29*, 7387−7401.

Dellwo, M. J., & Wand, A. J. (1989) *J. Am. Chem. Soc. 111*, 4571−4578.

Farrow, N., Zhang, O., Szabo, A., Torchia, D. A., & Kay, L. E. (1995) *J. Biomol. NMR 6*, 153−162.

Gitti, R., Long, G., & Bush, C. A. (1994) *Biopolymers 34*, 1327−1338.

Hajduk, P. J., Horita, D. A., & Lerner, L. E. (1993) *J. Am. Chem. Soc. 115*, 9196−9201.

Hricovini, M., & Torri, G. (1995) *Carbohydr. Res. 268*, 159−175.

Ishima, R., & Nagyama, K. (1995) *J. Magn. Reson. B108*, 73−76.

Jarvet, J., Allard, P., Ehrenberg, A., & Graslund, A. (1996) *J. Magn. Reson. B111*, 23−30.

Kay, L. E., Torchia, D. A., & Bax, A. (1989) *Biochemistry 28*, 8972−8979.

Kowaleski, J., & Widmalm, G. (1994) *J. Phys. Chem. 98*, 28−34.

Lefevre, J. F., Dayie, K. T., Peng, J. W., & Wagner, G. (1996) *Biochemistry 35*, 2674−2686.

Lipari, G., & Szabo, A. (1982a) *J. Am. Chem. Soc. 104*, 4546−4559.

Lipari, G., & Szabo, A. (1982b) *J. Am. Chem. Soc. 104*, 4559−4570.

Maler, L, Widmalm, G., & Kowalewski, J. (1996) *J. Biomol. NMR 7*, 1−7.

Markus, M., Dayie, K. T., Matsudaira, P., & Wagner, G. (1996) *Biochemistry 35*, 1722−1732.

McCain, D. C., & Markley, J. L. (1986) *J. Am. Chem. Soc. 108*, 4259−4264.

Peng, J. W., & Wagner, G. (1992) *J. Magn. Reson. 98*, 308−332.

Poppe, L., & vanHalbeek, H. (1992) *J. Am. Chem. Soc. 114*, 1092−1094.

Poppe, L., van Halbeek, H., Acquotti, D., & Sonnino, S. (1994) *Biophys. J. 66*, 1642−1652.

Press, W. H., Flannery, B. P., Teukolsky, S. A., & Vetterling, W. T. (1989) *Numerical Recipes in C*, Cambridge University Press, Cambridge, U.K.

Rutherford, T. J., Partridge, J., Weller, C. T., & Homans, S. W. (1993) *Biochemistry 32*, 12715−12724.

Schurr, J. M., Babcock, H. P., & Fujimoto, B. S. (1994) *J. Magn. Reson. B105*, 211−224.

Sklenar, V., Torchia, D. A., & Bax, A. (1987) *J. Magn. Reson. 73*, 375−379.

Stone, M. J., Fairbrother, W. J., Palmer, A. G., Reizer, J., Saier, M. H., & Wright, P. E. (1992) *Biochemistry 31*, 4394−4406.

Xu, Q. W., & Bush, C. A. (1996) *Biochemistry 35*, 14521−14529.

Xu, Q. W., Mohan, S., & Bush, C. A. (1996a) *Biopolymers 38*, 339−353.

Xu, Q. W., Gitti, R., & Bush, C. A. (1996b) *Glycobiology 6*, 281−288.

Yamazaki, T., Muhandiram, R., & Kay, L. E. (1994) *J. Am. Chem. Soc. 116*, 8266−8278.